Langmuir monolayers with internal dipoles: Understanding phase behavior using Monte Carlo simulations

Christopher B. George,[1,a)] Mark A. Ratner,[1] and Igal Szleifer[1,2]
[1]*Department of Chemistry, Northwestern University, Evanston, Illinois 60208, USA*
[2]*Department of Biomedical Engineering, Northwestern University, Evanston, Illinois 60208, USA*

(Received 15 October 2009; accepted 8 December 2009; published online 6 January 2010)

A coarse-grained, rigid-rod model that includes steric interactions and an internal dipole is used to study monolayers of surfactant molecules tethered to a flat interface. Monte Carlo simulations are performed in the canonical ensemble for a range of high-density configurations with varying degrees of dipole strength. Both a melting transition and a tilting transition are observed, and the dependence of the transitions on the surfactant molecules' internal dipoles is examined. Simulation results indicate that at high packing densities, the monolayers exist in a frustrated state due to dipole-dipole repulsions and steric interactions. Tilting of the surfactant molecules increases the magnitude of the dipole-dipole attractions and lowers the overall system energy, but is limited by steric repulsions. In simulations with higher dipole strengths, the melting and tilting transitions are found to be coupled. The formation of nanodomains with increased collective tilt and positional order in these systems suggests a possible mechanism for the coupling. © *2010 American Institute of Physics*.
[doi:10.1063/1.3280389]

I. INTRODUCTION

Monolayers of organic films formed on liquid surfaces have attracted increased attention recently due to their potential uses in a wide variety of technological applications. Langmuir monolayers can serve as precursors to Langmuir–Blodgett films, which have been used in applications ranging from electro-optic devices to biochemical sensors.[1] Molecular electronic junctions constructed from Langmuir monolayers on mercury have been formed as well, suggesting a potential route for creating and characterizing molecular electronic devices.[2] Langmuir films have also proven vital in more fundamental scientific studies such as understanding the physics of quasi-two-dimensional (2D) matter or the properties of biomembranes. A common theme linking the aforementioned applied and basic scientific studies is the importance of understanding, and in some cases controlling, the internal organization and phase behavior of Langmuir monolayers.

Several theoretical and experimental works have been conducted in order to achieve this aim.[3] A myriad of simulation studies have sought to elucidate the rich phase behavior of monolayers composed of amphiphiles, examining the roles of factors such as head group size, chain length, and chain flexibility.[4,5] Most simulation studies have employed coarse-grained models to represent the amphiphiles, tailored to include only the interactions and degrees of freedom that are deemed most critical for understanding the phase behavior in question. The present study adopts a similar strategy.

Of interest in this work is the interplay between short-range steric interactions due to van der Waals forces and long range interactions due to dipole-dipole forces. While previous works have primarily examined pattern formation and unique phase behavior due to dipole-dipole interactions between the hydrophilic head groups of amphiphiles,[6] additional dipole-dipole interactions are possible in Langmuir monolayers. For example, in semifluorinated *n*-alkanes $F(CF_2)_n(CH_2)_mH$, the dipoles arising from the CF_2-CH_2 junction, as well as the terminal CF_3 and CH_3 groups contribute to a significant overall dipole.[7] This dipole is expected to affect the packing as well as the phase behavior of Langmuir monolayers composed of fluorocarbon-hydrocarbon diblocks. Additionally, in Langmuir films formed on mercury, it has been shown that it is possible to modulate the total dipole moment of the constituent molecules by changing the chemical derivatization within the tail group.[8] Again, differences in the phase diagram stemming from different dipole moments would be expected.

In order to describe the general behavior of Langmuir monolayers composed of molecules with internal dipoles without attempting to model a specific surfactant, we use a coarse-grained model that includes both steric and electrostatic interactions. The high-density regime is probed, and tilting transitions, as well as a 2D melting process are observed and characterized using a range of order parameters. Results indicate that the system exists in a frustrated state at high densities due to dipole-dipole repulsions and steric interactions. Collective tilting of the model surfactant molecules is found to lower the overall potential energy of the system by allowing molecules to experience greater dipole-dipole attractions, but such tilting is limited by steric effects. The melting and tilting transitions are observed to be coupled in certain regimes, and the interplay between the two is discussed in detail. Metastable states are discussed briefly as well.

a)Electronic mail: c-george@u.northwestern.edu.

II. COMPUTATIONAL DETAILS

A. Model details

A rigid rod model with four Lennard-Jones centers is used to describe the surfactant molecules that compose a monolayer grafted to an interface. The Lennard-Jones potentials are truncated and shifted resulting in purely repulsive interactions. Each rod contains equal positive and negative charges located on the second and third Lennard-Jones spheres, respectively (Fig. 1); head and end monomers are uncharged. The four monomers are equally spaced along the rod with a distance of 0.67σ separating them. Steric interactions between monomers on different chains are described by

$$U_{\mathrm{LJ}}(r_{ij}) = \begin{cases} 4\varepsilon_{\mathrm{LJ}}\left[\left(\frac{\sigma}{r_{ij}}\right)^{12} - \left(\frac{\sigma}{r_{ij}}\right)^{6}\right] - 4\varepsilon_{\mathrm{LJ}}\left[\left(\frac{\sigma}{r_c}\right)^{12} - \left(\frac{\sigma}{r_c}\right)^{6}\right] & : \text{for } r_{ij} \le r_c \\ 0 & : \text{for } r_{ij} > r_c, \end{cases} \tag{1}$$

where $\varepsilon_{\mathrm{LJ}}$ provides a measure of the "hardness" of the repulsive potential, σ is the range of the Lennard-Jones potential, and r_{ij} is the distance between the monomers. The cutoff radius is $r_c = 2^{1/6}\sigma$. This choice effectively removes the attractive part. Coulomb interactions between monomers on different chains are described by

$$U_C(r_{ij}) = \frac{q_i q_j e^2}{4\pi\varepsilon_s r_{ij}}, \tag{2}$$

where e is the fundamental unit of charge, q_i and q_j are the number of charges on the two monomers (in units of e), and ε_s is the static permittivity of the system.

The head group monomer in a chain is defined as the Lennard-Jones center in contact with the xy plane ($z=0$). This monomer is restricted to translations in the xy plane, while the rest of the rod is allowed to rotate such that all other monomers remain above the xy plane ($z>0$). The $z=0$ surface is flat and completely insulating: no electrostatic response occurs due to the presence of the charges above the plane.

Our model has been designed to provide insight on the effects of internal dipoles on tilt order and translational order in monolayers of surfactant molecules. Because the only attractive interactions in the model are due to Coulomb forces, observed tilting transitions may be attributed to long range electrostatic forces as opposed to attractive Lennard-Jones interactions studied in other works.[5,9–11] Repulsive interactions between rods due to dipole-dipole forces also have a dramatic effect on the translational order. At high densities, rods are unable to completely minimize their electrostatic energy because tilting is inhibited by steric interactions. This results in a frustrated system with charge-dependent translational order.

The choice of a rigid chain as opposed to a flexible one reflects our interest in studying high density configurations in which intrachain conformational entropy is expected to be much less dominant in determining monolayer structure. Consequently, certain liquid-liquid phase transitions that depend upon intrachain entropy will not be observed with our model.[11,12]

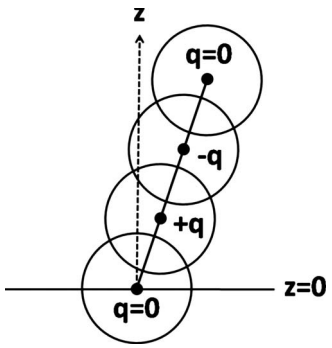

FIG. 1. A rigid rod, coarse-grained model with internal electric dipole. The head monomer is confined to translate in the xy plane, while the tail is allowed to rotate above the surface.

B. Simulation details

We perform off-lattice canonical Monte Carlo simulations with 1024 rods in a rectangular simulation cell with dimensions ($L_y/L_x = \sqrt{3}/2$) designed to accommodate hexagonal packing. In each trial move, a single rod is randomly selected and a translation or rotation move is performed (the choice of which is also random). The sizes of the rotation and translation steps are adjusted independently to maintain a Metropolis acceptance ratio of 0.5 for each type of move. Periodic boundary conditions are implemented in the x and y directions, and Coulomb interactions are truncated at $L_y/2$.

Dimensionless units are chosen using $\sigma=1$ and $e^2/4\pi\varepsilon_s=1$. In these units, the reduced temperature is defined as

$$T^* = \frac{4\pi\varepsilon_s\sigma kT}{e^2} = \frac{\sigma}{l_b} = \frac{1}{l_b^*}, \tag{3}$$

where l_b is the Bjerrum length. The strength of the steric repulsion between monomers is dictated by $\varepsilon_{\mathrm{LJ}}$, which is set to be $\varepsilon_{\mathrm{LJ}} = kTl_b^*$.

Simulations were performed over a range of densities ($\rho\sigma^2 = \rho^* = 0.7-0.95$) for several different charge strengths ($q=0-1.5$), all with $T^* = l_b^* = 1$. In each simulation, the rods were initially positioned vertically in a hexagonally packed configuration. An initial 500 000 Monte Carlo steps (MCS)

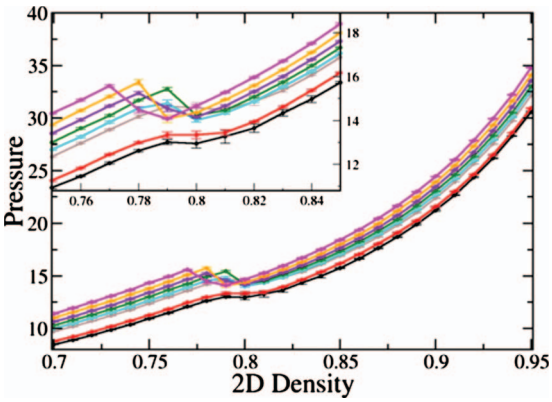

FIG. 2. Surface pressure in units of kTl_b/σ^3 vs density in units of σ^2 at constant temperature for $q=0$ (black), $q=0.5$ (red), $q=1.0$ (brown), $q=1.1$ (cyan), $q=1.2$ (green), $q=1.3$ (violet), $q=1.4$ (orange), and $q=1.5$ (magenta). Inset shows transition region.

were performed to equilibrate the system, followed by another 500 000 MCS with data collected every 500th MCS. One Monte Carlo step is defined as N attempted moves, where N is the number of rods in the system.

III. RESULTS AND DISCUSSION

Surface pressure-density isotherms are shown in Fig. 2 for simulations run with different charge strengths. The surface pressure is calculated using the virial theorem[13]

$$\Pi = \frac{NkT}{A} + \frac{1}{2A}\left\langle \sum_{i=1}^{N}\sum_{j>i} \boldsymbol{f}(\boldsymbol{r}_{ij})\cdot\boldsymbol{r}_{ij}\right\rangle, \tag{4}$$

where i runs over all rods, $\boldsymbol{f}(\boldsymbol{r}_{ij})$ is the force between two rods, and $\boldsymbol{r}_{ij}$ is the distance between the centers of mass of the rods. The isotherms in Fig. 2 indicate the presence of a phase transition occurring near $\rho^*=0.77-0.81$, where the transition density depends on the strength of the rods' charges. As the charge strength increases, the transition density drops to lower values.

A. Melting transition

A melting transition similar to those studied in 2D (Ref. 14) is partly responsible for the observed kinks near $\rho^*=0.80$ seen in Fig. 2. The transition occurs as particles in a disordered state are compressed until they are forced to pack hexagonally. The Langmuir monolayers studied here are nearly 2D; the head monomers may be understood as 2D particles with the rotation of the tail monomers acting as an internal degree of freedom. Consequently, the order-disorder transition may be characterized using order parameters utilized in 2D melting studies, namely, a local bond orientation order parameter defined as

$$\psi_{6,i} = \frac{1}{n_i}\sum_{j=1}^{n_i} e^{i6\theta_{ij}}, \tag{5}$$

where the sum on j runs over the nearest neighbors of particle i, the number of nearest neighbors is defined as n_i, and θ_{ij} is the angle between the line connecting head monomers i and j and an arbitrary axis.[14] The number of nearest neighbors of monomer i is computed by counting the number of head monomers that lie within a distance determined by the position of the first peak in the system's radial distribution function of head monomers, defined by[15]

$$g(r) = \frac{A}{2\pi r N^2}\left\langle \sum_i \sum_{j\neq i} \delta(r - r_{ij})\right\rangle. \tag{6}$$

Here r_{ij} is the distance between head monomers i and j, and N is the number of rods.

Additionally, the melting transition may be characterized via a bond orientation correlation function

$$g_6(r) = \left\langle \frac{\psi_6(r)\psi_6^*(0)}{\sum_i \sum_{j\neq i} \delta(r - r_{ij})}\right\rangle, \tag{7}$$

where

$$\psi_6(r) = \sum_i^N \delta(r - r_i)\psi_{6,i}. \tag{8}$$

In Eq. (8), the sum on i runs over all N head monomers. A global bond orientation order parameter may be defined as well

$$\langle|\Psi_6|\rangle = \left\langle \left| \frac{1}{N}\sum_i^N \psi_{6,i}\right|\right\rangle. \tag{9}$$

Radial distribution functions as well as bond orientation correlation functions of the $q=0$ and $q=1.5$ systems are shown in Fig. 3. The onset of long range positional order is evident in both systems from plots of the radial distribution functions, and the bond orientation correlation functions clearly show a shift in the order-disorder transition densities from approximately $\rho^*=0.80-0.81$ in the uncharged system to $\rho^*=0.76-0.77$ in the $q=1.5$ system. The charge-dependence of the melting transition densities is also visible in plots of the $\langle|\Psi_6|\rangle$ order parameter (Fig. 4). The results in Fig. 4 show a sharp rise for all charge strengths at or below densities of $\rho^*=0.80$, indicative of an order-disorder transition of the head monomers. The dependence of the melting transition on electrostatic strength is evident for runs with charges of $q\geq 1.2$. In these cases, the order parameter rises at progressively lower densities as the charge increases in contrast to simulations with charges of $q\leq 1.1$, where the order parameter begins to jump in a similar density range ($\rho^*=0.79-0.80$) regardless of charge strength.

The dependence of the positional order on charge strength is to be expected given the large dipole-dipole repulsions that exist in the highly frustrated system: steric interactions force the rods to pack nearly upright in high density configurations, thus increasing the repulsive electrostatic forces between rods. The apparent existence of two regimes is not so easily explained, however. In order to understand why systems with charges of $q\leq 1.1$ have similar transition densities while simulations with $q\geq 1.2$ show a monotonic decrease in transition density as a function of increasing charge strength, it is necessary to examine the tilt order of the monolayers.

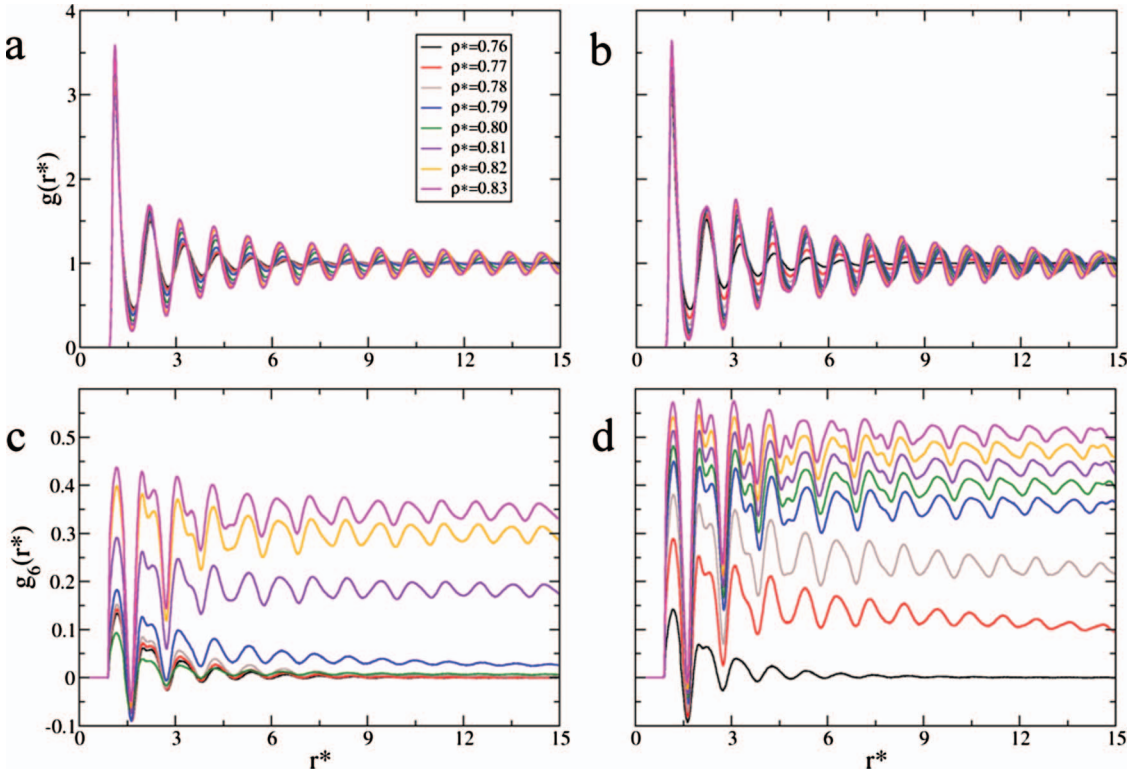

FIG. 3. Radial distribution functions $g(r^*)$ vs r^* in units of σ for head monomers with (a) $q=0$ and (b) $q=1.5$. Bond orientation correlation function $g_6(r^*)$ vs r^* in units of σ for head monomers with (c) $q=0$ and (d) $q=1.5$. Long-range order appears after the freezing transition. This transition occurs at lower densities for $q=1.5$ compared with $q=0$.

B. Tilting transition

The tilt order of the rods is described by $\langle \cos\theta \rangle$ where θ is the tilt angle of the rods from vertical, and by the normalized projection of the rods onto the xy plane given by

$$R_{xy} = \frac{\sqrt{\langle [x]^2 + [y]^2 \rangle}}{l}, \tag{10}$$

which is a measure of collective tilt. The x and y components of the projection are averaged over all the rods in a configuration and denoted by $[x]$ and $[y]$. The length of the rod is given by l. Values for the tilt order parameters are shown in Fig. 5. Systems with greater charge strengths exhibit greater tilt (lower $\langle \cos\theta \rangle$ values) at all densities demonstrating the propensity for charged systems to minimize their electrostatic potential energy by lying down and taking advantage of dipole-dipole attractions. As the monolayers are compressed, the rods are forced to stand upright due to steric interactions. For systems with charges, $\langle \cos\theta \rangle$ exhibits a dip as the density increases indicating the presence of a possible tilt transition. Evidence for a transition is also seen in the R_{xy} order parameter where the collective tilt jumps at different charge-dependent densities. Both the size of the increase in R_{xy}, as well as the shape of the curve are dependent on the charge strength, with the rise in R_{xy} becoming steeper and occurring at lower densities for higher charges. At a charge of $q=1.1$, the increase becomes nearly vertical and occurs at a density very close to the melting transition. Systems with charges of $q \geq 1.2$ show the same sharp increase in R_{xy} occurring at densities that become progressively lower.

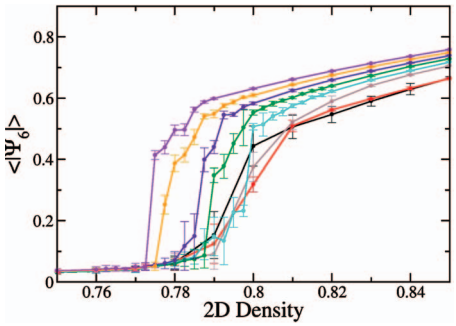

FIG. 4. Order parameter $\langle |\Psi_6| \rangle$ vs density in units of σ^2 for $q=0$ (black), $q=0.5$ (red), $q=1.0$ (brown), $q=1.1$ (cyan), $q=1.2$ (green), $q=1.3$ (violet), $q=1.4$ (orange), and $q=1.5$ (magenta). The melting transition occurs at approximately the same density for $q \leq 1.1$, while moving to lower densities for $q \geq 1.2$.

Comparing the plots in Figs. 4 and 5 suggests a coupling between tilting and melting transitions in systems with charges larger than $q=1.1$, and decoupled transitions for weaker charges. This coupling is similar to that observed in earlier works where tilting transitions caused by Lennard-Jones attractions were coupled to head group order in simulations of coarse-grained models.[5,9] In our study, the tilting transitions appear to drive the melting transition to lower densities after the two are coupled. Unlike the melting transition in systems with charges of $q \leq 1.1$ (in which all systems experience an increase in head group order at approximately the same density), the tilting transitions in simulations with higher charge occur at different densities.

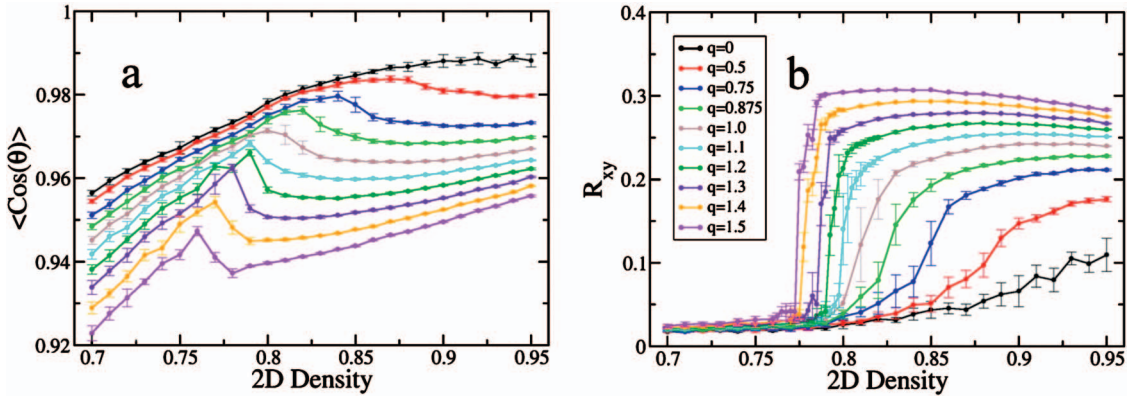

FIG. 5. Measures of tilt order (a) $\langle \cos\theta \rangle$ and (b) R_{xy}. Increased tilt (smaller $\langle \cos\theta \rangle$ values) is visible in systems with greater charge strengths. Dips in $\langle \cos\theta \rangle$ and jumps in R_{xy} indicate tilt transitions.

As the tilting transition density approaches the melting transition density at $q=1.1$, the transitions couple and both shift to lower densities for charges $q \geq 1.2$.

C. Coupled transitions

Of particular interest in this study is the mechanism of how phase transitions release frustration in a geometrically constrained environment. In order to search for and understand local domains within the monolayer structures at or near the melting transitions, local order parameters are calculated. Simulation boxes are discretized into 32×32 grids of equal sized bins (corresponding to one rod per bin on average), and order parameters are then calculated within each bin. The analog for Eq. (5) is then

$$\langle |\Psi_6| \rangle_a = \left\langle \left| \frac{1}{M} \sum_i^M \frac{1}{n_i} \sum_{j=1}^{n_i} e^{i6\theta_{ij}} \right| \right\rangle_a, \tag{11}$$

where the sum on i runs over all M monomers found within a particular bin a for a single configuration. The sums are then averaged over all values in a single bin yielding 1024 order parameters, one per bin. Similarly, the R_{xy} order parameter may be calculated within individual bins

$$(R_{xy})_a = \frac{\sqrt{[x]_a^2 + [y]_a^2}}{l}. \tag{12}$$

Here, $[x]_a$ and $[y]_a$ are the averages over all configurations of the x and y projections of rods within a particular bin a. A final measure of order is the average azimuth angle of the rods within a bin. This measure of tilt direction is calculated by finding the angle between the head-to-end vector projected on the xy plane and an arbitrary axis. The azimuth angle complements the R_{xy} order parameter by revealing if regions with collective tilt have the same average tilt direction as their neighbors. The local values of the three order parameters provide a means to visualize the formation of tilt domains and/or domains of head group order.

Representative samples of high-charge and low-charge systems are shown in Fig. 6. The color maps show values of the $\langle |\Psi_6| \rangle_a$ and $(R_{xy})_a$ order parameters, as well as the average azimuth angle for systems with charges of $q=0$ and $q=1.3$ and densities at the corresponding melting transitions ($\rho^*=0.798$ for $q=0$, $\rho^*=0.7875$ for $q=1.3$). The $q=0$ results indicate that there is negligible collective tilt on the surface, the melting transition occurs homogeneously across the simulation box, and the azimuth angles of the rods' tilts average to zero. The $q=1.3$ results paint a very different picture. A tilt domain forms with rods tilted in the same direction and the melting occurs nonhomogeneously. The rods within the tilt domain generally have higher local bond orientational order compared with the rods outside. This supports the earlier assertion that the two transitions are coupled at higher charge strengths and provides a possible mechanism as to how the melting transition occurs in systems with higher charge.

An important point to mention in the discussion of tilt domains and 2D melting is the role that finite size effects play in our results. We have not attempted to characterize the order of the melting transition due to the computational challenges associated with distinguishing between a solid phase and a hexatic phase. In purely 2D studies, it has been shown that very large simulations combined with a careful finite-size scaling analysis are necessary to distinguish between phases.[14,16] The radial distribution functions and bond orientation correlation functions in Fig. 3 indicate long-range positional order in our simulations, but our system size is too small to definitively claim a solid or hexatic phase. Similarly, the sizes and shapes of the tilt domains in our simulations are very likely affected by the finite size and fixed shape of the simulation cell. While the actual sizes of the tilt domains are unknown, the general mechanism of melting and the coupling between tilting transitions and melting transitions is expected to hold.

D. High density metastable states

Systems at high densities with strong charges may exhibit long-lived metastable states due to the frustrated nature of the system being studied. Steric repulsions combined with dipole-dipole repulsions lead to a frustrated system in which tilting is one of the few options to lower the overall potential energy. Consequently, tilt domains may form in which the system reaches a local energy minimum but cannot escape to the global minimum due to energy barriers imposed by repulsive interactions. Such behavior was observed in simula-

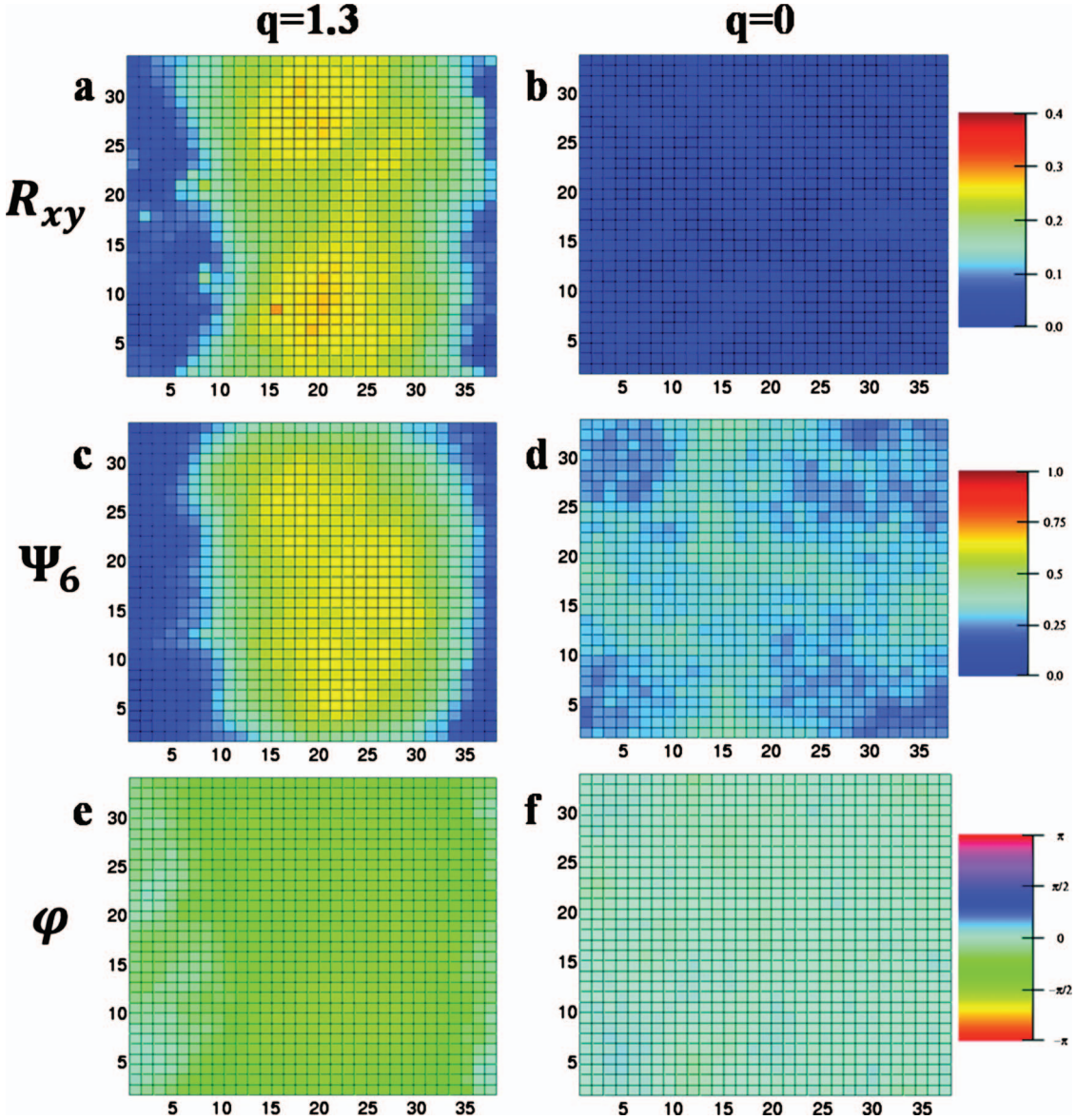

FIG. 6. Color maps of $(R_{xy})_a$ for (a) $q=1.3$ and (b) $q=0$, $\langle|\Psi_6|\rangle_a$ for (c) $q=1.3$ and (d) $q=0$, and azimuth angle φ for (e) $q=1.3$ and (f) $q=0$ at densities of $\rho^*=0.798$ for $q=0$, $\rho^*=0.7875$ for $q=1.3$. The selected densities correspond to the respective systems' melting transitions. The $q=1.3$ plots are representative of the analogous plots for systems with $q\geq 1.2$ at the melting transition, as are the $q=0$ plots for systems with $q\leq 1.1$. Axis labels are in units of σ.

tions with densities of $\rho^*=0.90$ and $\rho^*=0.92$ and charges of $q=1.5$. Results presented in Figs. 2 and 5 correspond to runs with identical parameters and initial configurations, but with final structures exhibiting homogeneous collective tilt and lower overall potential energies.

To understand the structure of the metastable states, color maps of R_{xy} and azimuth angles for the two systems are shown in Fig. 7. The local order parameters indicate that striped tilt domains form with both domains exhibiting collective tilt, but in opposite directions. It is likely that the size and shape of the domains are dependent on the size and shape of the simulation box. Configurations obtained from additional simulations exhibited uniform tilt (see Fig. 5) and had lower potential energies per rod with $U^*/N=4.11$ versus $U^*/N=4.37$ for $\rho^*=0.90$ and $U^*/N=4.52$ versus $U^*/N=4.82$ for $\rho^*=0.92$. The reduced potential energy per rod U^*/N is defined as $U^*/N=U/NkTl_b^*$, where N is the number of rods. While differences in the reduced energies are between 0.2 and 0.3, the kinetic barrier for relaxation between states is likely higher, resulting in long-lived metastable states.

IV. SUMMARY

Using Monte Carlo simulations, we have examined the melting transitions and tilting transitions of coarse-grained, rigid rod molecules containing an internal electric dipole. High density configurations have been studied in which a high degree of frustration is present due to repulsions resulting from steric and dipole-dipole interactions. Collective tilting releases some of this frustration by taking advantage of dipole-dipole attractions between rods. At higher dipole strengths, the melting and tilting transitions are found to couple. It is suggested that the tilting transitions drive the melting transitions to occur at lower densities. Results indicate that a possible mechanism for this coupling involves the

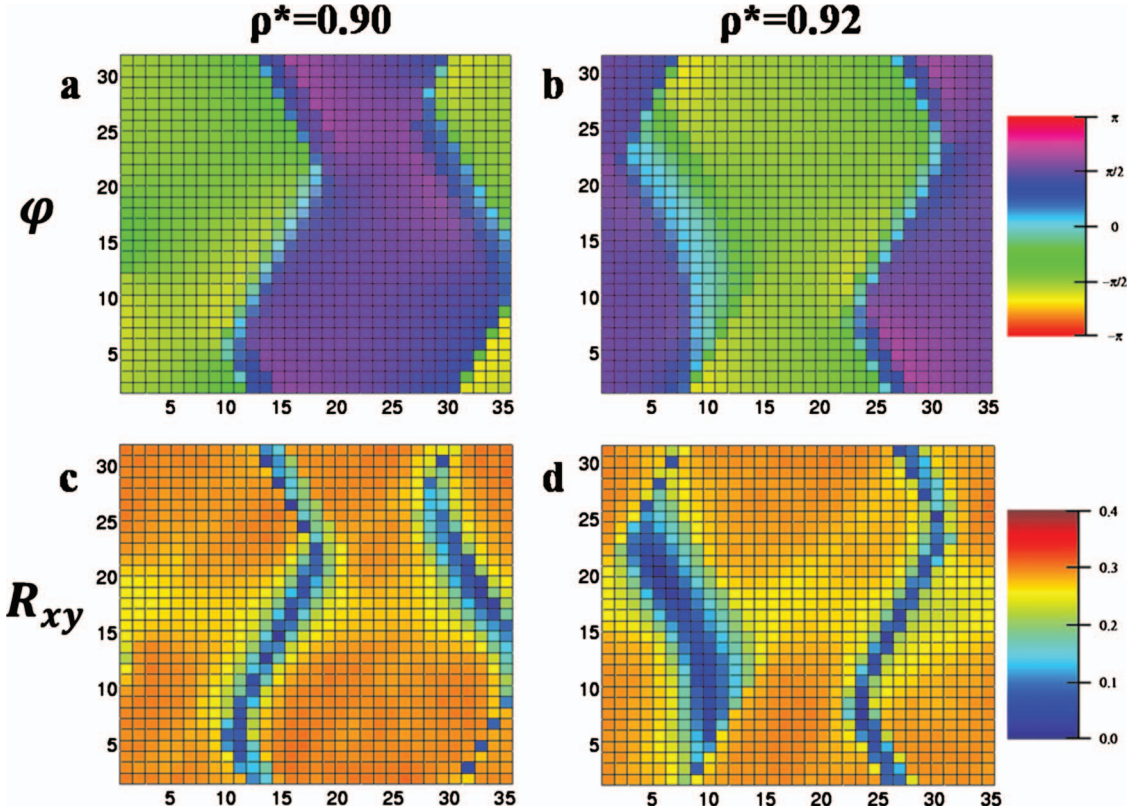

FIG. 7. Color maps of azimuth angle φ for (a) $\rho^*=0.90$ and (b) $\rho^*=0.92$ and $(R_{xy})_a$ for (c) $\rho^*=0.90$ (d) $\rho^*=0.92$ with charge of $q=1.5$. Plots of azimuth angle indicate the presence of two tilt domains in each simulation, and plots of the $(R_{xy})_a$ order parameters show that all tilt domains possess collective tilt. The presence of tilt domains in these systems results from the simulations becoming trapped in metastable states due to high densities and strong charges. Axis labels are in units of σ.

presence of domains with collective tilt and increased hexagonal order at densities near the melting transition. In systems with low charge, the tilting transition occurs at densities greater than the melting transition, and the melting transition is found to be relatively independent of charge strength.

Finite size effects are expected to alter the quantitative results, but the qualitative results are expected to remain the same. Investigations with larger system sizes may enable the determination of the order of the melting transition. The model could also be modified to include more realistic substrate interactions, greater chain flexibility, or more complicated molecular shapes, all of which would increase the complexity of the phase behavior.

At present, the model is general and attempts to provide insights on the competition between long and short range interactions in Langmuir monolayers. The results indicate that an internal electric dipole can serve as an additional knob with which to tune the phase behavior and structure of monolayers. Applications in which nanodomains with selective order are controlled by external electric fields may be envisioned. Such structural control of adsorbed and chemisorbed monolayers will be of the utmost importance as the field of interface engineering continues to grow at the nanoscale.

ACKNOWLEDGMENTS

This work is supported by the MRSEC program of the National Science Foundation (Contract No. DMR-0520513) at the Materials Research Center of Northwestern University. I.S. acknowledges financial support from the National Science Foundation through Grant No. CBET-0828046. C.B.G. is supported by a Graduate Research Fellowship from the NSF. The authors thank Marcelo Carignano for helpful discussions.

[1] A. Ulman, *An Introduction to Ultrathin Organic Films* (Academic, New York, 1991).
[2] R. E. Holmlin, R. Haag, M. L. Chabinyc, R. F. Ismagilov, A. E. Cohen, A. Terfort, M. A. Rampi, and G. M. Whitesides, J. Am. Chem. Soc. **123**, 5075 (2001); M. A. Rampi and G. M. Whitesides, Chem. Phys. **281**, 373 (2002).
[3] V. M. Kaganer, H. Mohwald, and P. Dutta, Rev. Mod. Phys. **71**, 779 (1999).
[4] D. Düchs and F. Schmid, J. Phys.: Condens. Matter **13**, 4853 (2001); S. B. Opps, B. Yang, C. G. Gray, and D. E. Sullivan, Phys. Rev. E **63**, 041602 (2001).
[5] C. Stadler and F. Schmid, J. Chem. Phys. **110**, 9697 (1999).
[6] H. M. McConnell and V. T. Moy, J. Phys. Chem. **92**, 4520 (1988); K. Thirumoorthy, N. Nandi, and D. Vollhardt, J. Phys. Chem. B **109**, 10820 (2005); Langmuir **23**, 6991 (2007).
[7] M. P. Krafft and J. G. Riess, Chem. Rev. (Washington, D.C.) **109**, 1714 (2009).
[8] L. Tamam, H. Kraack, E. Sloutskin, B. M. Ocko, P. S. Pershan, A. Ulman, and M. Deutsch, J. Phys. Chem. B **109**, 12534 (2005).
[9] F. M. Haas, R. Hilfer, and K. Binder, J. Chem. Phys. **102**, 2960 (1995).
[10] F. M. Haas, R. Hilfer, and K. Binder, J. Phys. Chem. **100**, 15290 (1996); C. Stadler, H. Lange, and F. Schmid, Phys. Rev. E **59**, 4248 (1999); D. R. Swanson, R. J. Hardy, and C. J. Eckhardt, J. Chem. Phys. **105**, 673 (1996).
[11] F. Schmid and M. Schick, J. Chem. Phys. **102**, 2080 (1995).
[12] S. W. Barton, A. Goudot, O. Bouloussa, F. Rondelez, B. H. Lin, F.

Novak, A. Acero, and S. A. Rice, J. Chem. Phys. **96**, 1343 (1992).
[13] D. Frenkel and B. Smit, *Understanding Molecular Simulation* (Academic, New York, 1996).
[14] K. J. Strandburg, Rev. Mod. Phys. **60**, 161 (1988).
[15] Here δ is the Kronecker delta function $\delta_{r,r_{ij}}$. Similar notation is used in Eqs. (7) and (8) for the Kronecker delta function.
[16] A. Jaster, Phys. Rev. E **59**, 2594 (1999); C. H. Mak, *ibid.* **73**, 065104 (2006).